

# Electrothermal design of DC busbars for fusion facilities

A. Cocchi <sup>a</sup>, G. De Marzi <sup>b</sup>, A. Lampasi <sup>b,c</sup>, R. Romano <sup>b</sup>

<sup>a</sup> *University of Rome Sapienza, Rome, Italy*

<sup>b</sup> *National Agency for New Technologies, Energy and Sustainable Economic Development (ENEA), Frascati, Italy*

<sup>c</sup> *DTT S.c. a r.l., Frascati, Italy*

The power supplies of nuclear fusion facilities are normally placed far (hundreds of meters) from the load coils and are connected to them through proper DC busbars. The design of such busbars is not trivial, as it must identify a tradeoff among different specifications. In this paper, the busbar electrothermal design is approached by specific tools and optimization criteria, taking into account the expected operating scenarios. The developed practical formulae, after being validated and extended by a finite-element method (FEM), were used to size the busbars according to the adopted criteria. It is interesting that different criteria are predominant in case of steady-state or pulsed busbars, leading to selection of different materials and configurations. The described algorithms were applied for the design of the busbar system of the DTT facility, but they can also be exploited in many applications and fields.

*Keywords:* DC busbar, Electrothermal analysis, Power supply, Convection, Irradiation, Multiphysics, Finite-element method (FEM), Divertor Tokamak Test (DTT)

## 1. Introduction

Fusion facilities as tokamaks are mostly based on high currents ( $\gg 1$  kA) flowing in coils to form the required magnetic fields. Mainly due to space and environmental constraints, the power supplies (PSs) generating and controlling such currents are placed far ( $>100$  m) from the load coils and are connected to them through proper busbars [1]. Such busbars are classified as DC because they are associated at the direct-current side of the PSs and operate differently from the standard electrical busbars in alternating currents.

The design of the DC busbars for such levels of currents and physical distances is not trivial, as the total losses may be in the order of tens of megawatts and the series parameters (resistance and inductance) can limit the PS performance. In fact, the series resistances reduce the voltage available on the load and the inductances affect the PS dynamic behaviors.

The design must identify a tradeoff among different requirements and constraints: voltage drops, operating temperature, electrodynamic stresses, current density, safety margins for faults, physical dimensions, layout, wall penetrations, environmental conditions, capital costs, operating costs (dissipated and cooling power) and so on. This paper is specifically focused on the electrothermal analysis, while the electromagnetic and structural analyses will be presented in a further work.

The design was approached by specific tools and optimization criteria, taking into account the operating scenarios expected for each busbar. The developed practical analytical formulae, after being validated by a finite-element method (FEM), were used to size the busbars according to the adopted criteria.

The described algorithms were applied for the design of the busbar system of the DTT facility [2], that is particularly demanding in terms of power density. The DTT busbars connect to the respective PSs: 6 modules for

the central solenoid (CS), 6 poloidal field (PF) coils, 3 blocks of 6 toroidal field (TF) coils in series, 2 in-vessel vertical stabilization (VS) coils, 4 in-vessel divertor (DIV) coils.

In DTT, the ex-vessel coils (CS, PF and TF) are superconducting, while in-vessel coils (VS and DIV) are made of copper. At the superconducting coil side, the DC busbars are terminated to special current leads that are interface between the connections at room temperature and the superconducting feeders at cryogenic temperature. Such feeders are cable-in-conduit-conductors cooled with forced flow of supercritical helium at a pressure around 5 MPa. The design of such feeders is in progress [3], while this paper is only focused on the room-temperature connections.

## 2. Basic input choices for the design

Some basic choices were preliminary adopted for practical reasons. The installation is totally indoor through specific tunnels. The busbars are rectangular, as sketched in Fig. 1, because this allows a good heat exchange, a simple design and it is the most common shape available on the market. The candidate materials for the busbars are copper (Cu) or aluminum (Al), but the latter should be preferred whenever possible to reduce costs. The use of water as coolant was excluded by the DTT project team, because it would require a deionization and pumping system, with reliability issues and possible safety hazards such as the circulation of activated water that must be stored in a special area [4]. Similarly, the forced air by cooling fans is only considered as a later option (in case of problems arising).

The design input is defined by the coil current scenarios and expected values [2, 5], as listed in Table 1 for all the DTT coils. Since DTT is conceived to be flexible to be adapted for different divertor configurations [2], the values in Table 1 are the worst cases for all the scenarios.

First, it is important to distinguish between pulsed and continuous busbars. In practice, only the 6 TF busbars belong to the latter category.

The pulsed busbars are expected to operate at full load for  $\approx 160$  s every hour, ten times a day [2]. For the pulsed loads, the thermal design is made considering two true root-mean-square (RMS) values of the current, computed only over the pulse period ( $I_{RMS160}$ ) and including the dwell time ( $I_{RMS3600} \approx I_{RMS160}/4.5$ ), respectively, as reported in Table 1.

Another relevant value for the design is the fault current, where two subcases were considered in Table 1: faults covered by the PS crowbar as quench of superconductors (maximum duration 20 s) [2, 5] and short-circuit between bars (1 s). The maximum current of each crowbar is well defined in its technical specifications [6]: in principle, it is the 10% more of the maximum coil current for the ex-vessel coils and 2-4 times the maximum coil current for the in-vessel coils, also depending on the coil position, number of turns and series inductance. The crowbar current is characterized by an exponential decay [6] with a time constant lower of 6 s in DTT [2], that is thermally much lower than 20 s at constant current. Also the duration considered for the short-circuit is a worst-case with respect to the expected values that are in the order of 100 ms. The estimation of the maximum short-circuit current is less immediate, but it is a common and reasonable practice to use a factor 5 with respect to the nominal current.

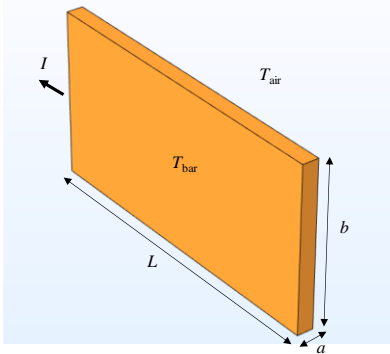


Fig. 1. Simplified sketch of a rectangular busbar.

Table 1. Expected characteristics of the DTT H&CD systems.

PS	$I_{max}$ (kA)	$I_{RMS160}$ (kA)	$I_{RMS3600}$ (kA)	$I_{crowbar}$ (kA)	$I_{short}$ (kA)
CS3U	25.9	13.9	3.1	35	150
CS2U	30.1	15.0	3.4	35	150
CS1U	31.3	21.3	4.8	35	150
CS1L	31.3	20.3	4.6	35	150
CS2L	31.3	18.8	4.2	35	150
CS3L	25.9	11.9	2.7	35	150
PF1	28.3	13.1	2.9	35	150
PF2	19.0	11.4	2.6	35	150
PF3	10.4	6.5	1.5	35	150
PF4	11.3	7.0	1.6	35	150
PF5	20.6	14.9	3.4	35	150
PF6	28.3	20.1	4.5	35	150
VS	5.0	3.0	0.7	20	150
DIV	25.0	13.5	3.0	60	150
TF	45.0	45.0	45.0	50	250

### 3. Analytical model of the power balance

The developed analytical model moves from the power balance on the rectangular busbar shown in Fig. 1:

$$P_{joule} + P_n + P_{EM} - P_{rad} - P_{conv} = \frac{dQ}{dt} = \rho c_p V \frac{dT_{bar}}{dt}. \quad (1)$$

Since this balance is virtually uniform over the bar length  $L$ , (1) can be considered on a unitary length. In order to apply (1) for the design, the following assumptions or models were introduced.

The power  $P_{joule}$  generated by Joule effect by the flowing current  $i$ . The nuclear heating  $P_n$  produced by neutron flux on a Cu bar was calculated to be  $\approx 200$  W/m<sup>3</sup> close to the cryostat and  $35 \div 80$  W/m<sup>3</sup> in the rest of the hall, which is negligible with respect to  $P_{joule}$  (that is at least 10 kW/m<sup>3</sup>). The electromagnetic heating  $P_{EM}$  due to the strong magnetic field originated by the tokamak coils and to the radiofrequency waves dispersed from the tokamak heating systems [2] can be locally significant, but can be neglected as the busbar path is mostly outside the tokamak hall.  $P_{rad}$  is the power lost by radiation from each bar surface  $S$ . The shape factor for each of these surface was assumed unitary. The solar radiation is not present due to the indoor installation, while the mutual heat radiation with the other objects is neglected. The power lost by convection  $P_{conv}$  is only related to the natural convection mechanism. The air temperature  $T_{air}$  is assumed constant at 35 °C, while the bar temperature  $T_{bar}$  can change but it is homogeneous within the bar.

Table 2. General parameters and air properties (at 35 °C) used in the model calculations.

Parameter description	Unit	Value
Density, $\rho$	kg·m <sup>-3</sup>	1.145
Thermal expansion coefficient, $\beta$	K <sup>-1</sup>	$3.28 \cdot 10^{-3}$
Thermal conductivity, $k_{air}$	W·m <sup>-1</sup> ·K <sup>-1</sup>	0.02625
Dynamic viscosity, $\mu$	kg·m <sup>-1</sup> ·s <sup>-1</sup>	$1.895 \cdot 10^{-5}$
Prandtl number, $Pr$	–	0.7268
Stephan-Boltzmann constant, $\sigma_{SB}$	W·m <sup>-2</sup> ·K <sup>-4</sup>	$5.67 \cdot 10^{-8}$

Table 3. Material properties and thermal constrains.

Description	Unit	Cu	Al
Density, $\rho$	kg·m <sup>-3</sup>	8890	2700
Specific heat, $c_p$	J·kg <sup>-1</sup> ·K <sup>-1</sup>	385.3	920
Thermal coefficient, $\alpha$	K <sup>-1</sup>	0.0038	0.004
Resistivity, $r_{20^\circ C}$	m $\Omega$ ·mm <sup>2</sup> ·m <sup>-1</sup>	17.8	28.6
Thermal conductivity, $k$	W·m <sup>-1</sup> ·K <sup>-1</sup>	390	290
Average emissivity, $\epsilon_m$	–	0.6	0.4
Max current density	A·mm <sup>-2</sup>	1.2	0.8
Max temperature, $T_{MAX}$	°C	80-90	60
Max temperature at fault	°C	200	120

Accordingly, the power in (1) derives from the sum of the following three contributions with the parameters summarized in Table 2 and Table 3:

$$P_{joule} = R(T)i^2 = \frac{L}{ab} \{r_{20^\circ} [1 + \alpha(T_{bar} - 293.15)]\} i^2, \quad (2)$$

$$P_{rad} = \sigma_{SB} \epsilon_m S (T_{bar}^4 - T_{air}^4), \quad (3)$$

$$P_{conv} = hS(T_{bar} - T_{air}). \quad (4)$$

A specific analysis is necessary for the (natural) convection coefficient  $h$  in (4). This can be calculated using the general heat theory based on dimensionless numbers Nusselt  $Nu$ , Grashoff  $Gr$  and Prandtl  $Pr$  [7]:

$$h = Nu \cdot \frac{k_{\text{air}}}{d_c} \quad (5)$$

The geometry of the system affects the characteristic dimension of the problem  $d_c$  and the dependence of  $Nu$  on the other two numbers. In particular,  $Nu$  depends on the considered surface, using for the top and bottom surfaces the convection coefficient for  $(Gr \cdot Pr) < 10^9$  [7]:

$$Nu = \begin{cases} 0.59 \cdot \sqrt[4]{Gr \cdot Pr} & \text{for the top surface,} \\ 0.27 \cdot \sqrt[4]{Gr \cdot Pr} & \text{for the bottom surface,} \\ [0.825 + 0.305 \sqrt[6]{Gr}]^2 & \text{for the lateral surfaces.} \end{cases} \quad (6)$$

## 4. Design criteria

An optimal busbar design must consider a tradeoff among different requirements. The output of the model is the selection of the bar material (Cu or Al) and the optimal bar cross-section meeting the selected design criteria. The identified criteria for the electrothermal design of the busbars are summarized in the following.

### 4.1. Steady-state criterion

The steady state criterion identifies the optimal cross-section imposing the maximum continuative temperature  $T_{\text{MAX}}$  during normal operations.

$$P_{\text{joule}} = P_{\text{conv}} + P_{\text{rad}} \quad (7)$$

### 4.2. Adiabatic criterion

The adiabatic criterion is conservative and can be applied only for the pulsed busbars, because they are heated for a short time. If the cooling mechanisms are totally neglected, the model (1) can be reduced to:

$$P_{\text{joule}} = \rho c_p V \frac{\Delta T_{\text{bar,max}}}{\Delta t_{\text{pulse}}} \quad (8)$$

In practice, the bar thermal constant will coincide with the pulse duration.

### 4.3. Fault criterion

In the fault criterion, all the heat generated during a fault must be completely absorbed by the busbar. The model is mathematically identical to the adiabatic one, but the current, time, and temperature values to be imposed in (8) are the fault values.

### 4.4. Current-density criterion

The current density criterion involves the use of the maximum current density ( $I/ab$ ) for the specific material imposed by material constrains. Even if this is not based on theoretical considerations, it is often used by the busbar manufacturers, with practical values suggested by the experience with real materials.

### 4.5. Maximum resistance criterion

This criterion imposes that the busbar resistance  $R(T_{\text{max}})$  defined in (2) should be lower than a predefined value, that was fixed to 1 mΩ. This resistance must be

fixed because is one of the main specifications for the PSs, both for the available voltage and for the energy losses. The voltage drop reduces the PS capability of controlling plasma, while the dissipated energy is more relevant for the energy-conservation converters adopted in DTT [5]. The same criterion could be equivalently expressed in terms of voltage drop, lost power or dissipated energy, by introducing  $I_{\text{max}}$  or  $I_{\text{RMS}}$ .

As evident in the formula (2), this is the only criterion requiring an assumption on the bar length  $L$ , while all the other criteria depend only on the properties of the bar cross-section.

### 4.6. Transient-time criterion

This criterion identifies the bar size that reaches the  $T_{\text{max}}$  of the material after a complete time evolution of (1). Due to the computational burden, this approach was rather used as a verification for the results obtained by the other criteria (as shown in Section 6).

## 5. Model results

The thermal design tool (design chart) resulting from the model is exemplified in Figs. 2-4 for a continuous (TF) and for a pulsed busbar (CSIU), the one with the highest maximum and RMS current). Each curve in the charts represents the optimal combination of  $a$  and  $b$  satisfying a specific design criterion. Since all the couples ( $a, b$ ) above the curves satisfy the criteria, the specific couple can be chosen by practical and economic considerations (as bar sizes available on the market).

Fig. 2 clearly shows that for the TF the size of a single bar would be impractical for both Cu and Al. A possible solution is to employ 2 bars per pole, each carrying 22.5 kA. As shown in Fig. 3, since the Al is impractical also in this case, the Cu must be selected as material. Anyway, in the final layout the TF PS was placed very close to the tokamak hall in order to limit the power losses.

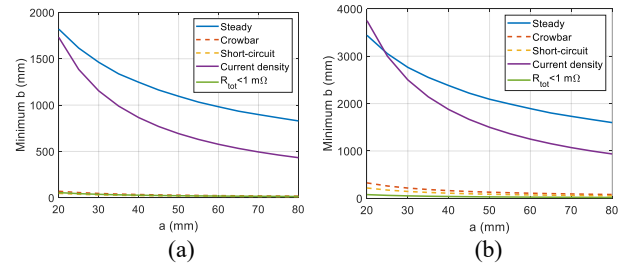


Fig. 2. TF design charts for a single bar and  $L=50$  m in the case of a bar made of Cu (a) and of a bar made of Al (b).

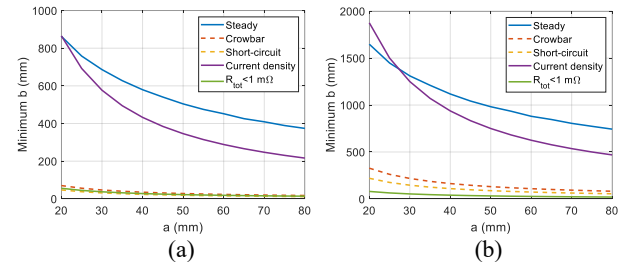


Fig. 3. TF design charts for one of two parallel bars carrying 22.5 kA and  $L=50$  m for the Cu (a) and Al (b) cases.

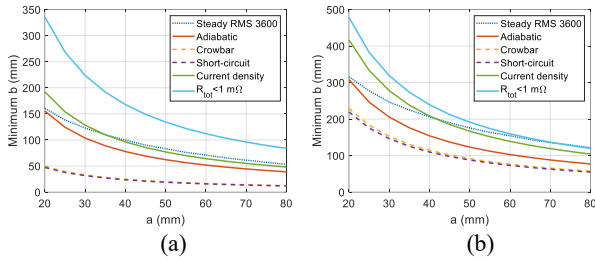


Fig. 4. CS design charts for  $L=300$  m for the Cu (a) and Al (b) cases.

Table 4. Preliminary design of the DTT busbar systems.

	TF	CS	PF	VS	DIV
Operations	Continuous			Pulsed	
Number of busbars	6	12	12	4	8
Material	Cu			Al	
Bars per pole	2			1	
Design criterion	Steady state	Maximum resistance			
$L$	$\approx 50$ m	$\approx 300$ m			
$a$	50 mm	40 mm			
$b$	500 mm	250 mm			

The preliminary design of the DTT busbars systems is summarized in Table 4, where the sizes were uniformed whenever possible. It is interesting to stress that different criteria result to be predominant in case of steady-state (steady-state criterion) or pulsed (maximum resistance criterion) busbars leading to selection of different materials and configurations.

It is interesting to notice that the use of the  $I_{RMS160}$  for the pulsed busbars would lead to a large oversizing of the design cross-section (about 4 times), for the same electrothermal performances, as shown in Fig. 5.

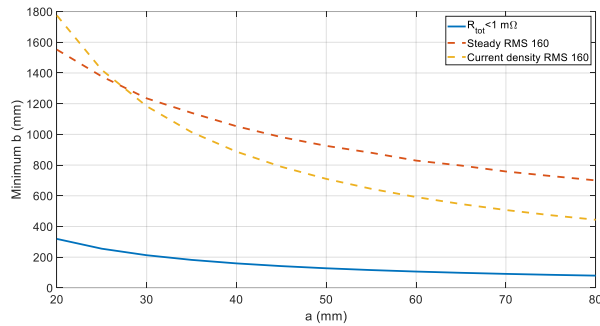


Fig. 5. CS design charts for Al in the same conditions of Fig. 4 but using  $I_{RMS160}$  instead of  $I_{RMS3600}$ . While the resistance criterion leads to the same curve, the new predominant criteria would lead to a large oversizing of the cross-section (about 4 times).

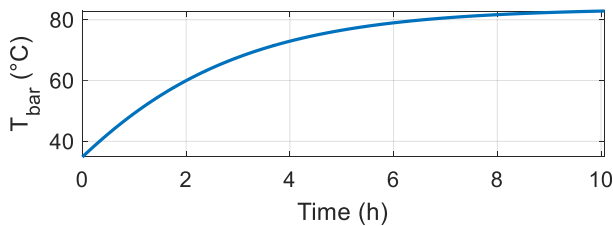


Fig. 6. Transient analysis for a TF Cu busbar (22.5 kA) with the selected design 50×500 mm.

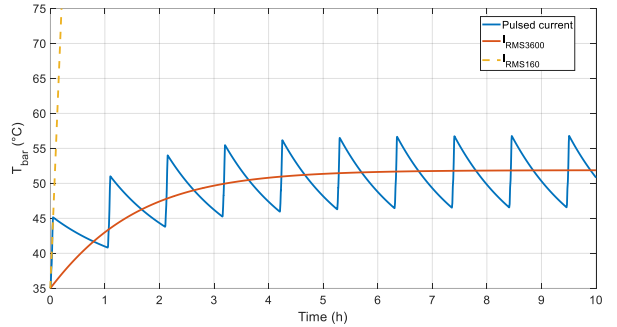
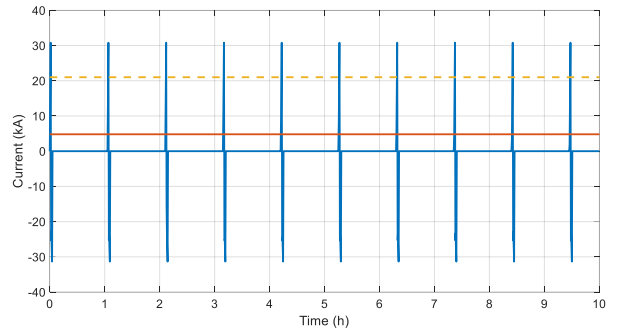


Fig. 7. Transient analysis for a CSIU Al busbar with the selected design 40×250 mm subject to the worst-case scenario. The analysis is performed for the actual current and for the equivalent RMS currents  $I_{RMS3600} \approx 4.8$  kA and  $I_{RMS160} \approx 21.3$  kA (the complete curve for the last case is not shown because it reaches almost 300 °C, well above the maximum continuative temperature of the material).

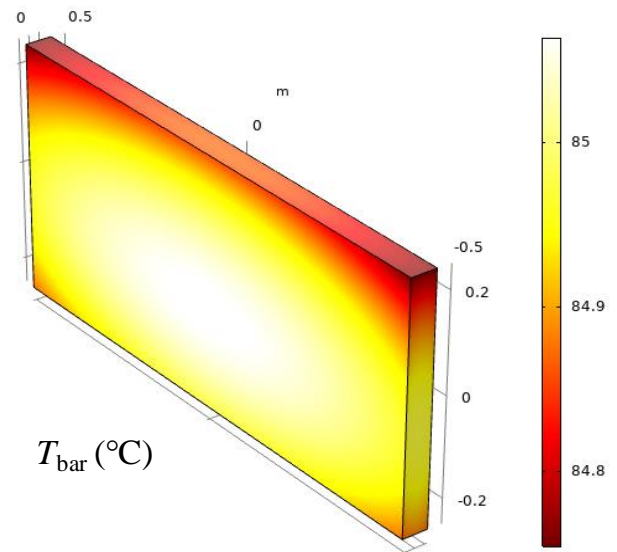


Fig. 8. Temperature distribution within a TF Cu busbar calculated by FEM analysis.

## 6. Verification by transient analysis

A transient analysis was carried out in order to verify the selected cross-section. The simulated temperature evolution of a TF busbar shown in Fig. 6 reaches a steady-state temperature of  $\approx 83$  °C, thus confirming the result of the analytical model.

Fig. 7 shows the transient thermal analysis for CSIU busbars considering a real-day operational scenario. The

results obtained for the actual pulsed (variable) current are compared with those that would be obtained for the equivalent RMS currents computed over the pulse period ( $I_{RMS160} \approx 21.3$  kA) and including the dwell time ( $I_{RMS3600} \approx 4.8$  kA), respectively. In the pulsed and  $I_{RMS3600}$  cases, the reached temperature is  $\approx 55^\circ\text{C}$ , that is below the continuous  $T_{MAX}$  admissible for the Al ( $60^\circ\text{C}$ ) because the adopted design criteria was the maximum resistance. On the other hand, it is confirmed that the use of  $I_{RMS160}$  is not adequate for the design of the pulsed busbars.

## 7. Validation by FEM analysis

The numerical thermal model developed is validated with a FEM analysis performed in the software environment COMSOL Multiphysics. The FEM model was implemented by coupling directly the fluid dynamics and the thermal field, without introducing empirical correlations, thus providing a model that is rather independent with respect to the analytical one, also removing the assumptions on  $T_{air}$  and  $T_{bar}$ .

The first interesting result is shown in Fig. 8 where it is possible to notice that the temperature distribution within a TF busbar can be considered uniform, confirming the assumption of the analytical model.

Fig. 9 compares the FEM and the analytical results for the same CS transient depicted in Fig. 7, showing a difference  $< 2^\circ\text{C}$  (also in this case,  $T_{bar}$  is rather uniform).

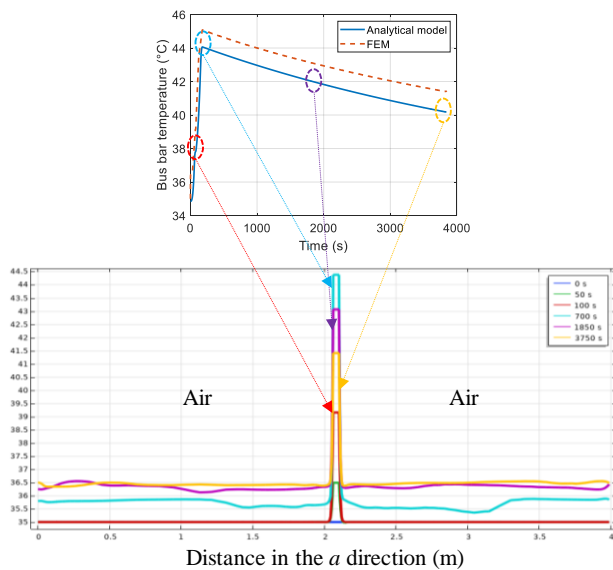


Fig. 9. Comparison between the curve in Fig. 7 and the results of the transient analysis performed by FEM on the same busbar inside a tunnel.

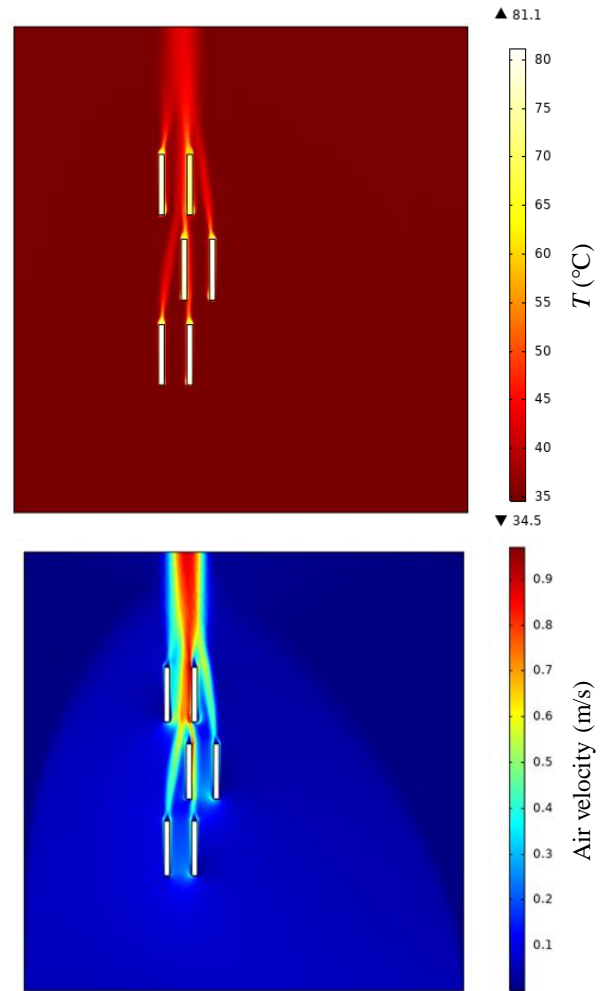


Fig. 10. Temperature and air velocity of an arrangement with 6 TF busbars.

The FEM approach allows to assess the effect of more bars including their configuration and layout (geometries, supports, enclosures and so on). An interesting case is shown in Fig. 10 considering 6 TF bars (having the same current). In this case, even though the heat is generated by multiple bars, the maximum temperature is lower than the case with a single bar (with same characteristics and current). This is due to the developed ascending natural air flow caused by the temperature difference between the busbars and the surrounding air inside the enclosure, as shown by the air velocity plot in Fig. 10.

## 8. Conclusions

This paper presented specific tools and optimization criteria for the design of the DC busbar of nuclear fusion facilities, using DTT as case study. These tools and criteria included analytical models, simplified and practical algorithms, and FEM simulations. Afterwards, the FEM was extended in order to verify the effect of several busbars.

The complete busbar system, including the layout optimization and the electromagnetic and structural analysis, will be the object of a forthcoming paper. The design of the busbar path is taking into account the problems related to the hall penetrations. In particular, the

busbars can access the tokamak hall only through proper doglegs in order to avoid direct exit paths for the neutrons [4]. This is expected to have a minor impact on the electrothermal design, because it could slightly increase the lengths of the bars, but not their cross-sections.

## References

- [1] F. Milani, J. Chiron, A. Roshal, V. Lokiev and R. Enikeev, "DC busbars for the ITER power supply system: Features and challenges," 2015 IEEE 26th Symposium on Fusion Engineering (SOFE), Austin, TX, 2015, pp. 1-6,
- [2] R. Martone, R. Albanese, F. Crisanti, P. Martin, A. Pizzuto "DTT Divertor Tokamak Test facility - Interim Design Report", ENEA, 2019.
- [3] G. De Marzi, et al., "Electromagnetic Analysis of the Superconducting Magnet Feeders System of the Divertor Tokamak Testing Facility", COMSOL Conference 2020 Europe, 14-15 October 2020.
- [4] R. Villari, et al., "Nuclear design of Divertor Tokamak Test (DTT) facility", Fusion Eng. and Design, Volume 155, 2020, 111551.
- [5] A. Lampasi, A. De Santis, S. Minucci, F. Starace, P. Zito, "Conceptual design of the power supply systems for the Divertor Tokamak Test facility", Fusion Eng. and Design, Volume 146, Part A, September 2019, pp. 937-941.
- [6] P. Zito, et al., "Design and testing of Crowbar Protection System for the JT-60SA superconducting magnet power supplies", Fusion Eng. and Design, Volume 124, November 2017, Pages 131-136.
- [7] R. T. Coneybeer, W. Z. Black, R. A. Bush, "Steady-state and transient ampacity of bus bar", IEEE Transactions on Power Delivery 9, 1994, 1822-1829.